THE JOURNAL OF PHYSICAL CHEMISTRY LETTERS
A JOURNAL OF THE AMERICAN CHEMICAL SOCIETY

pubs.acs.org/JPCL

Letter

Ultrafast Charge Relocation Dynamics in Enol–Keto Tautomerization Monitored with a Local Soft-X-ray Probe

Micheline B. Soley,[⊥] Pablo E. Videla,[⊥] Erik T. J. Nibbering, and Victor S. Batista*

Cite This: *J. Phys. Chem. Lett.* 2022, 13, 8254–8263

Read Online

ACCESS | Metrics & More | Article Recommendations | Supporting Information

ABSTRACT: Proton-coupled electron transfer (PCET) is the underlying mechanism governing important reactions ranging from water splitting in photosynthesis to oxygen reduction in hydrogen fuel cells. The interplay of proton and electronic charge distribution motions can vary from sequential to concerted schemes, with elementary steps occurring on ultrafast time scales. We demonstrate with a simulation study that femtosecond soft-X-ray spectroscopy provides key insights into the PCET mechanism of a photoinduced intramolecular enol* → keto* tautomerization reaction. A full quantum treatment of the electronic and nuclear dynamics of 2-(2′-hydroxyphenyl)benzothiazole upon electronic excitation reveals how spectral signatures of local excitations from core to frontier orbitals display the distinctly different stages of charge relocation for the H atom, donating, and accepting sites. Our findings indicate that ultraviolet/X-ray pump-probe spectroscopy provides a unique way to probe ultrafast electronic structure rearrangements in photoinduced chemical reactions essential to understanding the mechanism of PCET.

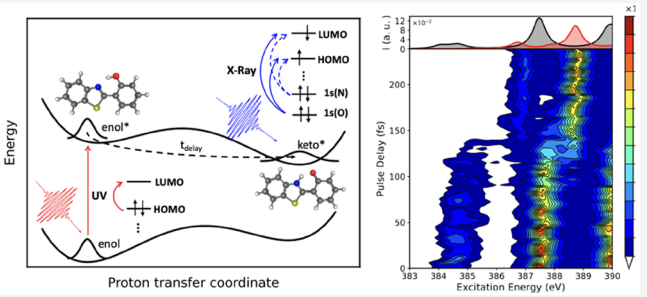

Understanding the dynamics of electronic rearrangements associated with proton transfer reactions remains a subject of great fundamental interest. Charge relocation is governed by the underlying microscopic mechanism generally known as proton-coupled electron transfer (PCET),[1−6] where the time scales for motions of electronic degrees of freedom (electronic charge distributions) and those of nuclear degrees of freedom (of the transferring proton and of hydrogen bond deformation modes) may be different or identical. PCET will then involve sequential or concerted reaction pathways, respectively. Examples in which PCET plays a key role include water splitting by photosystem II, nitrogen fixation, and oxygen reduction in biocatalysis and in hydrogen fuel cell technologies.[7−19] Significant molecular rearrangements induced by photoinduced proton transfer along preexisting hydrogen bonds have been reported for many years, going back at least to the pioneering work of Weller on derivatives of salicylic acid monitored by ultraviolet−visible (UV−vis) spectroscopy.[20,21] Since then, numerous studies have focused on understanding the process of photoinduced proton transfer in a variety of molecular systems, including hydroxyflavones, salicylaldehydes, 2-(2′-hydroxyphenyl)benzothiazole derivatives, and related molecules.[22−27] Nevertheless, probing the electronic rearrangements at the molecular level is a topic of intense research effort (see, for instance, refs 28 and 29 for recent advances in ultrafast X-ray scattering, ref 30 for soft-X-ray spectroscopy, and ref 31 for ultrafast electron diffraction). Here, we explore the capabilities of soft-X-ray ultrafast spectroscopy, as applied to the characterization of electronic dynamics during photoinduced intramolecular proton transfer in 2-(2′-hydroxyphenyl)benzothiazole (HBT), shown in Figure 1, as described by simulations of quantum dynamics, including a full quantum treatment of all nuclear degrees of freedom.

At the molecular level, proton transfer involves electronic density changes directly at the proton donor and acceptor sites and beyond the donating and accepting groups, including polarization of the molecule and surrounding solvent environment. The effect of the proton on the local electronic structure of functional groups involved in proton exchange—occurring on the femtosecond time scale before, during, and after the elementary proton translocation—is still rather unexplored from an experimental point of view. *Ab initio* molecular dynamics simulations have provided insights into proton transport in bulk solvents through the von Grotthuss mechanism[32−36] and acid dissociation dynamics.[37−40] In general, proton transfer and electron transfer are thermodynamically coupled, yet kinetics might determine the overall relaxation and time scales of electron and proton rearrangements. So, fundamental questions remain to be addressed,

Received: June 30, 2022
Accepted: August 18, 2022
Published: August 26, 2022

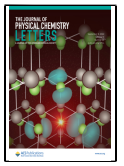

https://doi.org/10.1021/acs.jpclett.2c02037
J. Phys. Chem. Lett. 2022, 13, 8254–8263

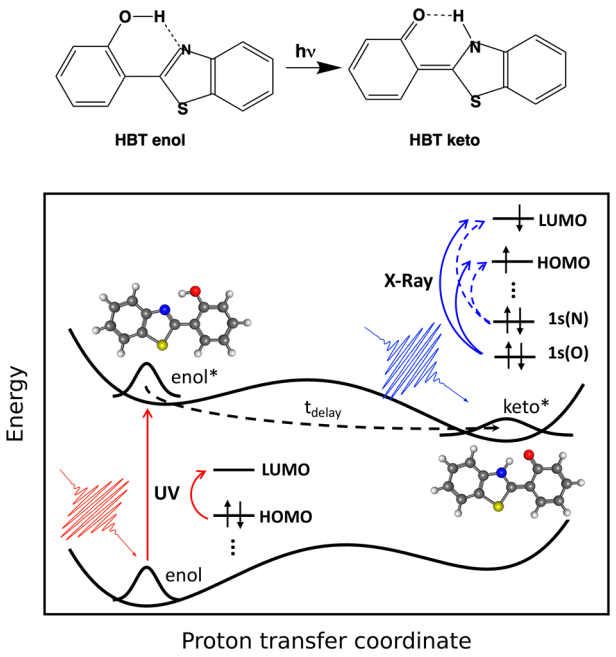

Figure 1. Schematic representation of pump−probe ultraviolet (UV)/X-ray spectroscopy to probe the HBT enol−keto tautomerization following photoexcitation (top). UV photoexcitation of the HOMO → LUMO transition initiates an ultrafast intramolecular proton transfer along the O−H···N hydrogen bond. A delayed soft K-edge X-ray pulse induces O/N 1s core → HOMO/LUMO transitions that probe transient electronic features of HBT.

including the following. Is a proton or a hydrogen atom transferred after photoexcitation? Is proton transfer driven by photoinduced electronic rearrangements? What electronic degrees of freedom are most critical for proton transfer, those of the donating or accepting groups? Moreover, what nuclear motions are critical for hydrogen bonding[41] and therefore essential for charge transfer events? Here, we address these fundamental questions in the study of electronic rearrangements due to enol−keto tautomerization in HBT after $S_0 \rightarrow S_1$ photoexcitation, which are dominated by the highest-occupied to lowest-occupied molecular orbital (HOMO → LUMO) transition that triggers intramolecular proton transfer along the intramolecular O−H···N hydrogen bond (Figure 1).

The photoinduced enol−keto conversion of HBT occurs on the ultrafast time scale, as monitored by UV−vis[42−44] and UV−infrared pump−probe spectroscopy.[45−49] Ultrafast spectroscopy has demonstrated that the molecular vibrations of HBT change in character when the C−O−H···N chemical bonds of the HBT-enol* state convert into the C═O···H−N configuration of the HBT-keto* state (the asterisk denotes the photoexcited state).[45−47,49] Furthermore, it was shown that low-frequency hydrogen bond modes are actively involved in the excited-state proton transfer reaction.[43,50] In fact, a particular form of PCET has been suggested to be an appropriate description because electronic structural rearrangements are concomitant with the proton transfer event.[49,51−53]

A combined study including polarization-resolved UV−infrared pump−probe spectroscopy and time-dependent density functional theory (TDDFT) has shown that only a small amount of net positive charge is transferred to the benzothiazole ring when *cis*-enol* converts into the *cis*-keto* tautomer.[49] In fact, the benzothiazole side of HBT acquires a charge difference of ∼0.34*e* (i.e., only 34% of a full proton transfer) upon excited-state enol−keto tautomerization, which suggests significant electronic rearrangements through the molecular framework that mostly neutralize the proton translocation. However, direct spectroscopic evidence of the underlying electronic rearrangements remains lacking.

Soft-X-ray spectroscopy provides unprecedented capabilities for probing the electronic structure of molecules undergoing photoinduced transformations with ultrafast and atomic (submolecular) resolution.[54−68] In recent years, major advances in steady-state and time-resolved soft-X-ray spectroscopy[69−76] include the development of liquid jet technologies for sample delivery[77] at dedicated end stations of large-scale facilities based on storage rings[78] and linear accelerators.[79] In addition, laser-based systems using extreme high-order harmonic generation of soft-X-ray pulses have become available.[80] Here, we analyze simulations of time-resolved X-ray absorption spectroscopy (TRXAS) to assess whether ultrafast soft-X-ray spectroscopy could provide a characterization of intramolecular PCET reactions.

Time-resolved XAS is particularly suitable for exploring PCET in HBT because it induces transitions of core electrons from 1s atomic orbitals localized on specific atoms involved in proton transfer to low-lying molecular orbitals (i.e., HOMO and LUMO) that are largely unaffected by PCET. Therefore, X-ray absorption provides access to changes in electronic states localized in proton donor and acceptor groups, which allows for ultrafast pump−probe schemes that can probe the evolution of the chemical reaction with atomic resolution.[68,81]

We focus on X-ray absorption spectroscopy using the K-edge absorption bands of nitrogen (N) and oxygen (O) to probe the transient electronic structure of HBT during the photoinduced enol−keto tautomerization induced by UV $S_0 \rightarrow S_1$ excitation. We follow the spectral signatures of O, while probing changes of its electronic environment, and N as it is protonated during formation of the keto product. We analyze the 1s → HOMO/LUMO transitions that can be probed by ultrafast X-ray absorption spectroscopy. We follow the detailed evolution of the electronic excited state coupled to nuclear dynamics, including bond-breaking and bond-forming events described by a full quantum treatment of all nuclear degrees of freedom.

Monitoring changes in the K-edge bands of O and N could capture the evolution of the electronic structure at the proton donor and acceptor sites. A rigorous interpretation of the nuclear and electronic rearrangements responsible for changes in the XAS spectra can be provided by simulations of quantum dynamics as described by the tensor-train split-operator Fourier transform (TT-SOFT) method.[82] TT-SOFT is a rigorous method for simulations of quantum dynamics that exploits matrix product-state representations analogous to those employed by recently developed methods for simulating vibrational and fluorescence spectroscopy[83−85] and other methods for simulations of quantum dynamics and global optimization.[86,87] In TT-SOFT, the initial nuclear wave function evolves according to the Schrödinger equation, and therefore, nuclear quantum effects, such as zero-point energy, delocalization, and interference effects, are naturally incorporated into the simulations. Whereas MCTDH[88] tensor network quantum dynamics relies on the hierarchical Tucker format and MCTDH equations of motion, TT-SOFT employs tensor trains and split-operator Fourier transform dynamics that facilitate simulation of highly multidimensional chemical

https://doi.org/10.1021/acs.jpclett.2c02037
J. Phys. Chem. Lett. 2022, 13, 8254−8263

systems and avoid ill-conditioned matrices (see also ref 89). Here, we demonstrate for the first time the capabilities of TT-SOFT as applied to simulations of UV/XAS pump−probe spectroscopy. We discuss how the UV and soft-X-ray pulse characteristics determine the outcome of an experiment, as could be implemented in state-of-the-art facilities that have become available in recent years.

Figure 2 shows the evolution of the proton transfer coordinate Q_{PT} associated with the enol−keto tautomerization,

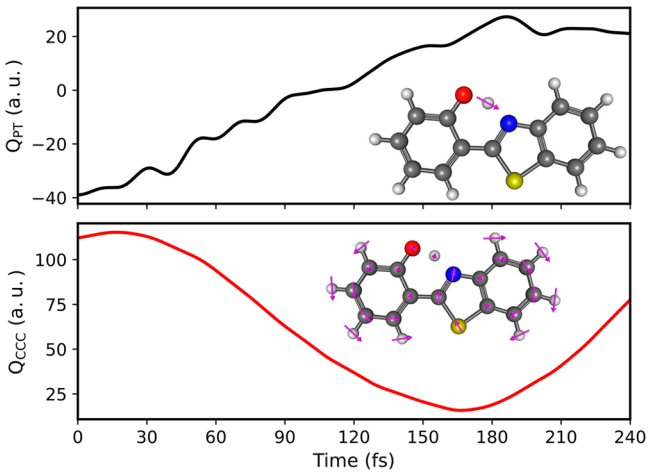

Figure 2. Dynamical evolution of the proton transfer (top) and CCC internal in-plane bending (bottom) large-amplitude modes after photoexcitation of HBT. Insets show the normal mode displacements associated with each coordinate.

as it converts OH···N to O···HN, as described by wave packet propagation on adiabatic *ab initio* full-dimensional potential energy surfaces computed at the TDDFT level of theory (see Computational Methods and the Supporting Information for additional computational details). Q_{PT} represents the (mass-weighted) normal mode displacement associated with the imaginary frequency at the transition-state (TS) configuration, for which $Q_{PT} = 0$ (see the inset of Figure 2), and allows one to distinguish enol-like ($Q_{PT} < 0$) from keto-like ($Q_{PT} > 0$) configurations. HBT starts in the enol* form, where the expectation value of the proton transfer coordinate is negative, and converts into the keto* form ($Q_{PT} \geq 0$) within 200 fs, in agreement with previous results suggesting excited-state intramolecular proton transfer (ESIPT).[49,90−92] The expected value of the proton transfer coordinate remains in the range of values corresponding to the keto* isomer for the remainder of the examined dynamics, consistent with previous findings suggesting equilibration within 400−600 fs of photoexcitation of the system.[91] Figure 2 also shows the time-dependent expectation value of the normal mode displacement associated with the CCC internal in-plane bending mode that modulates the N−O distance between the proton donor and acceptor moieties (see the inset of Figure 2), with an oscillation period of ∼250 fs, comparable to the time scale for proton transfer. The time-dependent population of the keto isomer is also consistent with the ultrafast time scale for keto* formation within 50 fs of photoexcitation of the system (see the Supporting Information).

The reported quantum dynamics simulations are in good agreement with earlier studies, which supports the accuracy of our TT-SOFT simulations. UV−vis pump−probe measurements have demonstrated that the enol* → keto* reaction dynamics of HBT is strongly governed by low-frequency Raman-active modes that are impulsively excited by the electronic enol → enol* transition.[43,44,92−94] In particular, the in-plane 255 cm^{-1} mode plays a key role, as it modulates the O−H···N hydrogen bond distance and, thus, the reaction coordinate along which the H atom is transferred (see Figure 2). The observed time scale for the enol* → keto* reaction dynamics has been ascribed to nuclear motions that in particular comprise this low-frequency mode, which compels photoexcited HBT to proceed on the excited-state potential energy surface with a major excursion along this nuclear coordinate. A further refinement to this picture can be made, given that additional pump−probe signal modulations have been ascribed to low-frequency modes at 113, 289, and 528 cm^{-1}. As our TT-SOFT method estimates the propagation dynamics of HBT in a full quantum treatment, our results can show the extent to which these low-frequency Raman-active modes play a key role in the wave packet dynamics in the enol* → keto* reaction dynamics and how these modes influence the femtosecond UV/XAS spectroscopic observables during the chemical reaction.

Panels a and b of Figure 3 compare the simulated steady-state X-ray absorption near-edge structure (XANES) spectra of HBT in the S_0 and S_1 electronic states, which correspond to the K-edge of nitrogen (Figure 3a) and oxygen (Figure 3b), respectively. The S_0 spectrum of N is characterized by an intense pre-edge peak centered at 387.9 eV and a broad band at ∼390.6 eV. Analysis of the natural transition orbitals (NTOs) shows the lower-energy peak corresponds mainly to the 1s(N) → LUMO transition (with small contributions from higher π^* orbitals), whereas the higher-energy band is dominated by the 1s core excitation to a delocalized π^* orbital centered on the thiazole ring (Figure 3a, inset). The O XANES spectrum, shown in Figure 3b, is characterized by two main peaks located at 520.2 and 521.7 eV that arise from 1s core excitations from the 1s(O) orbital to the LUMO and a delocalized π^* orbital centered on the hydroxyphenyl ring, respectively. Notice that given the delocalized, extended, and π character of the valence molecular orbitals, which involve contributions from both O and N atoms, the lowest-energy transitions in both N and O spectra correspond to transitions to the same final state (i.e., 1s → LUMO), whereas higher-energy transitions reach excited states that are localized on different rings as determined by differences in the cross sections of the 1s core excitations to the respective final states. We note that contributions from double excitations are neglected by the single-reference MOM/TDDFT method used in this work and are expected to contribute to the high-energy region of the spectra so they would require more advanced electronic structure calculation methods. The calculated ground-state XANES spectra compare favorably in terms of spectral features and peak positions with the O and N K-edge spectra of related compounds with a similar local bonding environment, including 10-hydroxybenzo[*h*]-quinoline,[95] 2-mercaptopyridine,[96] uracil,[65] and malonaldehyde.[97]

Changes in electronic character induced by the $S_0 \rightarrow S_1$ UV photoabsorption can be identified in the XANES spectra. Panels a and b of Figure 3 show the spectra corresponding to 1s core transitions immediately after UV photoexcitation of the molecule to the S_1 excited state in the enol configuration (red lines). New pre-edge features dominated by the 1s core →

https://doi.org/10.1021/acs.jpclett.2c02037
J. Phys. Chem. Lett. 2022, 13, 8254−8263

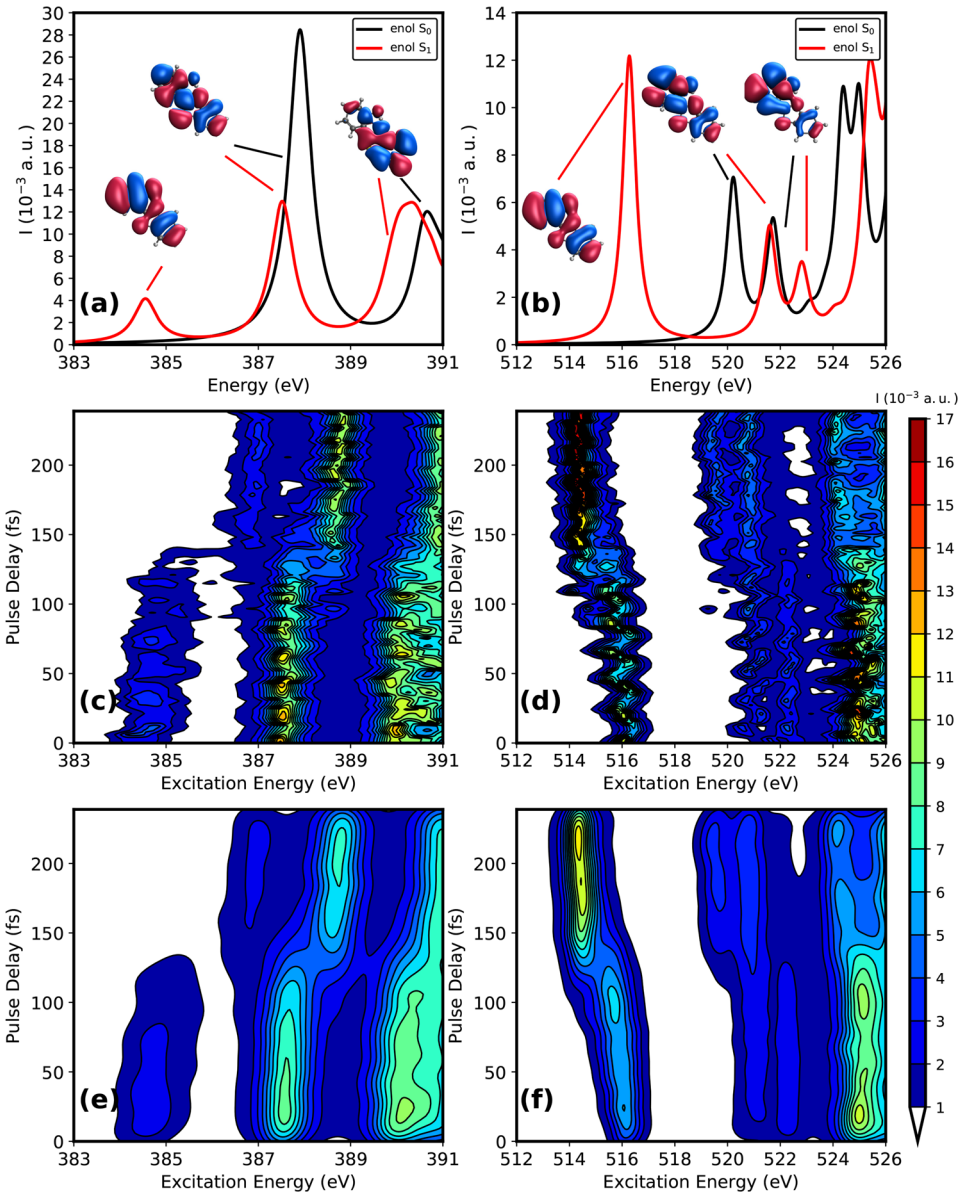

Figure 3. (a) Nitrogen K-edge and (b) oxygen K-edge XANES spectra for HBT in the enol tautomer in the S_0 ground state (black line) and the subsequent photoexcitation to the Franck−Condon region of the enol* S_1 excited state (red line). Stick spectra were convoluted with Lorentzian functions with a 500 meV full width at half-maximum (fwhm). The inset shows the dominant NTOs of the 1s core excitation (isovalue of 0.02). (c) Nitrogen K-edge and (d) oxygen K-edge TRXAS following photoexcitation. Instrumentally convoluted (e) nitrogen K-edge and (f) oxygen K-edge TRXAS. A Gaussian instrumental response function with effective temporal and spectral resolution fwhms of 20 fs and 0.5 eV, respectively, was used in accordance with experimentally available X-ray free electron lasers and tabletop HHG setups.

HOMO transition are observed at 384.6 and 516.3 eV for the N and O K-edge, respectively. That well-resolved single peak feature arises from the vacancy of the HOMO created by the pump (see Figure 1) and provides a distinct spectroscopic fingerprint of the electronic excited state. We remark that, because both N and O atomic orbitals contribute to the formation of the delocalized HOMO orbital, the N and O pre-edge transitions reach the same final state, corresponding to 1s → HOMO transitions arising from the 1s(N) and 1s(O) orbitals, respectively. The spectral shifts between these pre-edge peaks, therefore, correspond to the relative energy between 1s N and O orbitals (*vide infra*) because the final state is the same for the N and O pre-edge features. Rearrangements of the electronic density induced by the S_0 → S_1 photoexcitation also change the peak positions and intensities of the remaining XANES bands. Note that the N 1s core → LUMO transition is red-shifted by 0.4 eV, whereas an ∼1 eV blue-shift is observed for the O atom 1s core → LUMO transition. These results suggest that the 1s core → HOMO/LUMO transitions of N and O provide valuable probes of the electronic excited state of the enol* tautomer.

Panels c and d of Figure 3 show transient X-ray absorption spectra computed after photoexcitation of the enol HBT tautomer, which provides evidence of the ability of TRXAS to probe the electronic structural changes during the photo-induced proton transfer dynamics. The transient spectra are computed from the full quantum mechanical wave packet corresponding to an initial vibrational ground state that is instantaneously excited to the S_1 electronic state (see Computational Methods and the Supporting Information).

https://doi.org/10.1021/acs.jpclett.2c02037
J. Phys. Chem. Lett. 2022, 13, 8254−8263

The nitrogen K-edge TRXAS (Figure 3c) provides clear fingerprints of nuclear dynamics in the S_1 excited state. A significant blue-shift (1−2 eV) is observed for the 1s core → HOMO/LUMO transitions of HBT in the enol* conformation upon comparison of the 0 fs delay time to the keto* conformation at 200 fs and beyond. The disappearance of peaks at 384.5 and 387.5 eV and the concomitant appearance of the peaks at 387 and 389 eV provide spectral signatures of the enol* → keto* transformation, predicted to occur in 100−150 fs, in excellent agreement with theory and earlier experiments.[49,90−92] Note that the time scale of the photoisomerization coincides with the minimum amplitude of the CCC bending mode (Figure 2), which is consistent with the key role of the low-frequency reaction coordinate in regulation of the proton transfer dynamics. The TRXAS spectra also show that the peak positions and intensities oscillate with a period of approximately 20−24 fs, which suggests a tuning mode with a frequency of 1400−1700 cm^{-1}, within the frequency range of O−H and N−H bending modes. Resonance Raman spectra of HBT show that modes involved in aromatic ring C−C and C═C deformation and the O−H bending mode overlap in that spectral range, with intensities corresponding to pronounced displacements along those modes induced by the electronic excitation.[94] Therefore, both of those modes are excited by the UV pump pulse and modulate the transient absorption spectrum, as shown in Figure 3, which provides a detailed characterization of the photoisomerization process by UV/XAS pump−probe spectroscopy. Similar features are observed in the oxygen K-edge TRXAS spectrum (Figure 3d). Both the 1s core → HOMO and 1s core → LUMO transition frequencies exhibit a 1−1.5 eV shift on the time scale of 100−150 fs, which provides spectroscopic evidence of the ultrafast isomerization process with subpicosecond resolution. These observations provide key insights into the dynamics of electronic structural rearrangements during the enol* → keto* tautomerization process.

We remark that these results are in agreement with recent observations from a classical *ab initio* simulation of the PCET process in the related 10-hydroxybenzo[*h*]quinoline (HBQ) molecule,[95] where clear X-ray spectral signatures of coupled electronic and atomic motions were observed at the oxygen and nitrogen K-edge. Whereas HBQ presents a rigid framework that delimits changes in the O−N distance, in HBT the O−N fluctuations are crucial in modulating the proton transfer process (*vide supra*). Interestingly, for HBQ, the 1s-to-HOMO transition is visible for only the O K-edge, whereas HBT presents the pre-edge features in both N and O spectral regions. In this regard, HBT provides two independent spectroscopic probes that can be experimentally used to track excited-state dynamics, paving the way for future experiments at X-ray free electron laser facilities.

Figure 4 shows that the frontier orbitals remain largely unaffected by the enol−keto tautomerization. Furthermore, Figure 4 compares the time evolution of the HOMO and LUMO energies to the energies of 1s atomic orbitals of N and O during the isomerization dynamics. The time-dependent orbital energies provide a fundamental understanding of the dynamical features of TRXAS probing the enol* → keto* isomerization. In effect, because the pre-edge transitions correspond to 1s core → HOMO/LUMO transitions, spectral shifts for those transitions report directly on changes in the frontier orbital energies relative to the 1s core atomic orbital energies, which in turn are modulated by the changes in

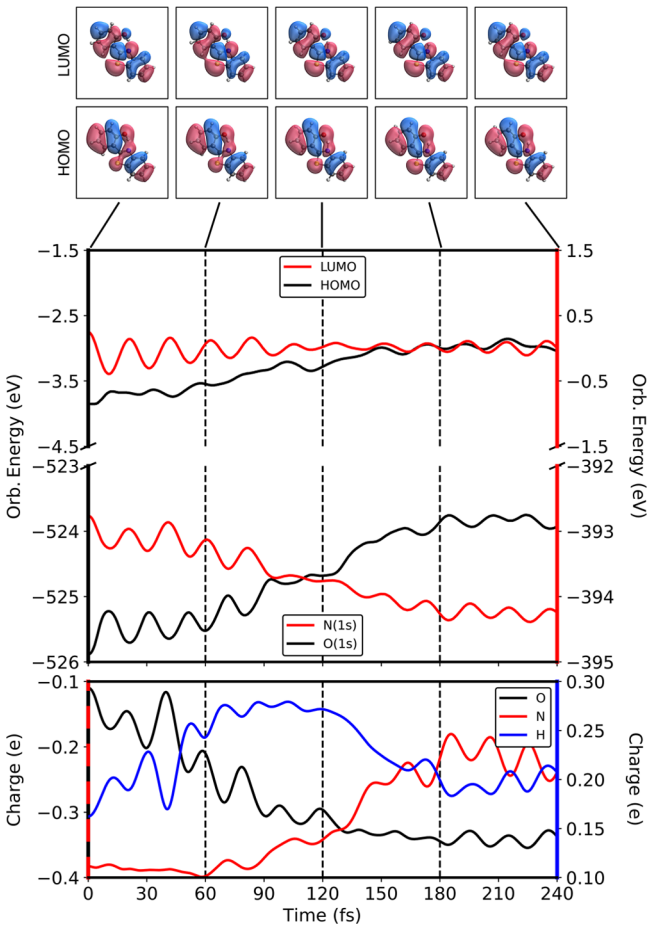

Figure 4. Time evolution of the HOMO/LUMO and core 1s orbital energy of O and N atoms (top). Time evolution of the Mulliken charges on the O, N, and transferring H atoms (bottom). Note the different scales of the data (as indicated by the colored border of the axis). Insets at the top show the HOMO and LUMO frontier orbitals, which indicate subtle changes during the enol* → keto* tautomerization reaction (isovalue of 0.02).

electrostatic potential during the tautomerization process. Remarkably, the 1s core orbitals exhibit a significant energy shift, whereas changes in the frontier orbital energies are much smaller. Therefore, the resulting shifts report on localized changes in the electronic structure and electrostatic potential of the chromophore with submolecular (atomic) spatial resolution.

We find that the enol−keto tautomerization stabilizes the N 1s orbital and destabilizes the O 1s core level, in excellent correlation with the observed changes in the N and O K-edge TRXAS peaks, which become blue- and red-shifted, respectively (Figure 3c,d). In addition, Figure 4 shows that changes in the energy levels of the HOMO and LUMO frontier orbitals, which play a key role in the excited-state ultrafast tautomerization, are rather subtle. Similar findings have been reported for 2-(2′-hydroxyphenyl)benzotriazole[98,99] and methylsalicylate.[100]

The time-dependent Mulliken charges, displayed in Figure 4, indicate that changes in the core orbital energies are correlated with the rearrangement of electronic charges induced by the enol* → keto* tautomerization. The O negative charge increases (in magnitude) during the tautomerization process, whereas the N atom becomes more neutral. The increase in

https://doi.org/10.1021/acs.jpclett.2c02037
J. Phys. Chem. Lett. 2022, 13, 8254−8263

electronic density around the O atom destabilizes the 1s orbital, which leads to a smaller energy gap between the 1s core orbital and the delocalized frontier orbitals. The opposite is observed for the N atom. As such, the blue- and red-shifts of the N and O K-edge TRXAS peaks, shown in panels c and d of Figure 3, can be traced back to changes in the electronic charge distribution and electrostatic potential induced by the tautomerization reaction.

Figure 4 shows transient changes in the charge on the transferring H as the OH bond is broken and the NH bond is formed. H becomes most positive halfway through the transfer process (at ∼120 fs) before the N−H bond is formed. That intermediate stage exhibits a strong attenuation of the pre-edge spectral peak. The N 1s core → HOMO TRXAS signal recovers only after the N−H bond is formed, which demonstrates the sensitivity of the TRXAS peak intensities to electronic reorganization dynamics, in addition to the previously discussed energy shifts. Therefore, we find that the evolution of the TRXAS spectra can probe the detailed dynamics of intramolecular proton-coupled electron transfer,[49] including changes in the electronic environment of the proton donor and proton acceptor functional groups within 200 fs. We remark that the total charge on the benzothiazole and hydroxyphenyl ring along the isomerization process follows trends similar to those of the charge on O and N, respectively (see the Supporting Information).

Figures 3 and 4 show the sensitivity of the nitrogen and oxygen K-edge XAS bands to the dynamics of intramolecular electronic rearrangements due to the tautomerization of HBT, assuming infinite instrumental resolution. In practice, on the basis of recent major advances in steady-state and time-resolved soft-X-ray spectroscopy both at X-ray free electron laser facilities and with tabletop HHG setups,[69−73,75,76,78−80] we anticipate spectrometer devices might offer an effective temporal resolution of 20 fs and spectral resolutions of 0.5 eV. In panels e and f of Figure 3, we present the convoluted TRXAS spectra assuming a Gaussian instrumental response profile. Clearly, with that limited resolution, the fastest nuclear coherences of fingerprint vibrational modes would be averaged out. Nevertheless, the essential, dominant contribution of the hydrogen bond modulation mode that governs the time scale of the enol* → keto* conversion at ∼120 fs would remain clearly discernible. Hence, we anticipate that experiments that probe transient electronic structural dynamics of PCET can provide unique insights beyond the capabilities of conventional ultrafast spectroscopic methods.

In conclusion, we have investigated the ability of time-resolved X-ray absorption spectroscopy at both the nitrogen and oxygen K-edge to resolve the ultrafast enol-to-keto isomerization photophysics in HBT upon photoexcitation. We find that TRXAS can resolve the long-standing question of whether the photoinduced HBT tautomerization proceeds via excited-state PCET or intramolecular hydrogen transfer. The reported simulations show that UV pump−soft-X-ray probe spectroscopy can probe the nitrogen and oxygen K-edge bands to provide a detailed characterization of the ultrafast dynamics of electronic structural rearrangements during the photo-induced enol* → keto* tautomerization of HBT. The reported results show that the main driving force of the reaction results from electronic structural rearrangements initiated by UV photoexcitation. The electronic excitation triggers relaxation of nuclear coordinates through a sequence of stages, starting with displacement of the CCC internal bending bond and bringing together the proton donor (OH) and proton acceptor (N) functional groups. The resulting displacement polarizes the O−H bond by strengthening the OH···N hydrogen bond, which increases the positive atomic charge of H and the negative atomic charge of O and partially reduces the negative atomic charge of N by delocalization through conjugated double bonds within 120 fs of HBT photoexcitation (Figure 4). The proton is then transferred and forms a covalent bond with N. The resulting changes in electronic density change the bond order of proton donor/acceptor groups and cause the evolution of the hydroxyphenyl and benzothiazole rings into resonance structures corresponding to the keto isomer.

We have shown that the TT-SOFT dynamics simulates the nuclear motion, including quantum delocalization, of the transferring proton through the low-barrier hydrogen bond of the S_1 state, while the MOM/TDDFT method resolves the electronic transitions of TRXAS. Therefore, the combination of TT-SOFT and MOM/TDDFT methods has allowed us to track both electronic and nuclear rearrangements fully quantum mechanically and resolve the PCET nature of the reaction mechanism. The methodology is quite general and applicable to a wide range of molecules beyond HBT. Chemical systems amenable to TT-SOFT simulations are widespread, including other reactive coordinate systems with quantum baths and hydrogen bonding in DNA base pairs, water molecules, and Zundel cations. Therefore, we anticipate that TT-SOFT/MOM simulations of pump−probe spectra can provide valuable interpretations of UV pump−X-ray probe spectra of chemical processes in which analogous dynamics of electronic and nuclear rearrangements determine the time scale and nature of reaction mechanisms as well as the outcome of photoinduced reactions.

PCET for HBT is not fully concerted, but rather sequential, with charge relocations occurring on distinctly different times for the oxygen-donating atom, the inner proton, and the nitrogen-accepting atom. Initially, during the first 120 fs of the PCET process, when the O···N distance is shortened due to the internal bending motion between the hydroxyphenyl and benzothiazole units and the H atom has transferred halfway, electronegative charge density at the oxygen atom increases while that of the inner H atom decreases (making it more positive). In the next 120 fs of the PCET process, the O···N distance is lengthened again, the H atom electronegative density increases, and that of the nitrogen atom decreases. These results show the interplay among charge relocation, hydrogen bond modulation motions, and proton motion. These results are expected to be highly relevant for other PCET processes, and ultrafast soft-X-ray spectroscopy will be a highly valuable tool for discerning the different steps in PCET.

■ COMPUTATIONAL METHODS

Full-dimensional *ab initio* ground- and excited-state potential energy surfaces were parametrized at the (TD)-DFT level of theory employing the ωB97XD functional[101] and cc-pvdz basis set,[102] as implemented in Gaussian 16.[103] Solvent effects were included implicitly through the PCM polarizable continuum model,[104−108] using dichloromethane to mimic PCET of HBT dissolved in nonpolar solvents, which can be properly described with an implicit solvent model. Explicit modeling of the solvent would be necessary for simulations in protic polar solvents, which can be involved in hydrogen bonds with the O and N atoms. We expect that the main findings of our study should remain qualitatively insensitive to the type of

https://doi.org/10.1021/acs.jpclett.2c02037
J. Phys. Chem. Lett. 2022, 13, 8254−8263

solvent provided they are nonpolar and have similarly low dielectric constants. To reduce the computational cost associated with the PES parametrization, we employed a reaction surface approach[109−111] in which two reactive coordinates (namely, the proton transfer and CCC bending coordinate) are explicitly parametrized, whereas the other 67 degrees of freedom are treated as harmonic. Additional information regarding the parametrization can be found in the Supporting Information.

The dynamics of HBT following photoexcitation were described in terms of wave packet propagation on the adiabatic full-dimensional potentials with the TT-SOFT method.[82] Nonadiabatic effects (conical intersections and non-Born−Oppenheimer effects) were neglected. For the ultrafast femtosecond short time scales involved in the PT process studied here, and given the picosecond time scales involved in the excited-state lifetime,[112] we expect this approximation to be valid for short periods.[113] Future work will focus on the inclusion of nonadiabatic effects and their effect on transient X-ray spectroscopy. Tensor-train manipulations are performed with Oseledet's TT-Toolbox for the fast interpolation procedure[114] via the cross approximation.[115] We have made the codes available in the public domain.[89]

The X-ray transition energies and dipole strengths for HBT in the excited state were obtained following our previous work[68] by a combined maximum overlap method (MOM)[116,117] and TDDFT[118] approach as implemented in the Q-Chem package.[119] The MOM strategy was used to obtained the S_1 electronic wave function, which was subsequently used as a reference state to perform TDDFT core excitations. All calculations were performed using the ωB97XD functional[101] and cc-pvdz basis set,[102] with dichloromethane employed as the implicit solvent through PCM.[104−108] Transient X-ray spectral line shapes are modeled as an incoherent superposition of core excitations weighted by the magnitude of the nuclear wavepacket at a given time instant according to Monte Carlo sampling. The spectral sticks were broadened with a Lorentzian envelope with full width at half-maximum of 0.5 eV to approximate the core−hole lifetime broadening of each atom and to take into account experimental resolution.

■ ASSOCIATED CONTENT

Supporting Information

The Supporting Information is available free of charge at https://pubs.acs.org/doi/10.1021/acs.jpclett.2c02037.

> Additional details about the methods and results, including the development of the potential energy surface, dynamics, and time-resolved UV pump−X-ray probe spectra; analysis of the fully quantum treatment dynamics; and evaluation of potential and spectrum approximations (PDF)

■ AUTHOR INFORMATION

Corresponding Author

Victor S. Batista − *Department of Chemistry, Yale University, New Haven, Connecticut 06520-8107, United States; Energy Sciences Institute, Yale University, West Haven, Connecticut 06516-7394, United States; Yale Quantum Institute, Yale University, New Haven, Connecticut 06520-8263, United States;* orcid.org/0000-0002-3262-1237; Email: victor.batista@yale.edu

Authors

Micheline B. Soley − *Department of Chemistry, Yale University, New Haven, Connecticut 06520-8107, United States; Yale Quantum Institute, Yale University, New Haven, Connecticut 06520-8263, United States;* orcid.org/0000-0001-7973-2842

Pablo E. Videla − *Department of Chemistry, Yale University, New Haven, Connecticut 06520-8107, United States; Energy Sciences Institute, Yale University, West Haven, Connecticut 06516-7394, United States;* orcid.org/0000-0003-0742-0342

Erik T. J. Nibbering − *Max Born Institute for Nonlinear Optics and Short Pulse Spectroscopy, 12489 Berlin, Germany;* orcid.org/0000-0001-5874-8052

Complete contact information is available at: https://pubs.acs.org/10.1021/acs.jpclett.2c02037

Author Contributions

[⊥]M.B.S. and P.E.V. contributed equally to this work.

Notes

The authors declare no competing financial interest.

■ ACKNOWLEDGMENTS

M.B.S. acknowledges financial support from the Yale Quantum Institute Postdoctoral Fellowship. V.S.B. acknowledges support from National Science Foundation Grant CHE-1900160 and high-performance computing time from NERSC. E.T.J.N. acknowledges support from the European Research Council (ERC) under the European Union's Horizon 2020 research and innovation programme (ERC Grant Agreement 788704, E.T.J.N.).

■ DEDICATION

This work is dedicated to Thomas Elsaesser for his contributions to ultrafast science in general and to ultrafast photoinduced intramolecular proton transfer processes in particular for more than four decades.

■ REFERENCES

(1) Huynh, M. H. V.; Meyer, T. J. Proton-Coupled Electron Transfer. *Chem. Rev.* **2007**, *107*, 5004−5064.

(2) Weinberg, D. R.; Gagliardi, C. J.; Hull, J. F.; Murphy, C. F.; Kent, C. A.; Westlake, B. C.; Paul, A.; Ess, D. H.; McCafferty, D. G.; Meyer, T. J. Proton-Coupled Electron Transfer. *Chem. Rev.* **2012**, *112*, 4016−4093.

(3) Mayer, J. M. Understanding Hydrogen Atom Transfer: From Bond Strengths to Marcus Theory. *Acc. Chem. Res.* **2011**, *44*, 36−46.

(4) Hammes-Schiffer, S.; Soudackov, A. V. Proton-Coupled Electron Transfer in Solution, Proteins, and Electrochemistry. *J. Phys. Chem. B* **2008**, *112*, 14108−14123.

(5) Hammes-Schiffer, S. Proton-Coupled Electron Transfer: Moving Together and Charging Forward. *J. Am. Chem. Soc.* **2015**, *137*, 8860−8871.

(6) Tyburski, R.; Liu, T.; Glover, S. D.; Hammarström, L. Proton-Coupled Electron Transfer Guidelines, Fair and Square. *J. Am. Chem. Soc.* **2021**, *143*, 560−576.

(7) Reece, S. Y.; Nocera, D. G. Proton-Coupled Electron Transfer in Biology: Results from Synergistic Studies in Natural and Model Systems. *Annu. Rev. Biochem.* **2009**, *78*, 673−699.

(8) Meyer, T. J.; Huynh, M. H. V.; Thorp, H. H. The Possible Role of Proton-Coupled Electron Transfer (PCET) in Water Oxidation by Photosystem II. *Angew. Chem., Int. Ed.* **2007**, *46*, 5284−5304.

(9) Costentin, C.; Robert, M.; Savéant, J.-M. Concerted Proton-Electron Transfers: Electrochemical and Related Approaches. *Acc. Chem. Res.* **2010**, *43*, 1019−1029.
(10) Crabtree, R. H. Multifunctional Ligands in Transition Metal Catalysis. *New J. Chem.* **2011**, *35*, 18−23.
(11) Gagliardi, C. J.; Vannucci, A. K.; Concepcion, J. J.; Chen, Z.; Meyer, T. J. The Role of Proton Coupled Electron Transfer in Water Oxidation. *Energy Environ. Sci.* **2012**, *5*, 7704−7717.
(12) Wenger, O. S. Proton-Coupled Electron Transfer with Photoexcited Metal Complexes. *Acc. Chem. Res.* **2013**, *46*, 1517−1526.
(13) Mora, S. J.; Odella, E.; Moore, G. F.; Gust, D.; Moore, T. A.; Moore, A. L. Proton-Coupled Electron Transfer in Artificial Photosynthetic Systems. *Acc. Chem. Res.* **2018**, *51*, 445−453.
(14) Warren, J. J.; Mayer, J. M. Moving Protons and Electrons in Biomimetic Systems. *Biochemistry* **2015**, *54*, 1863−1878.
(15) Wang, T.; Brudvig, G.; Batista, V. S. Characterization of Proton Coupled Electron Transfer in a Biomimetic Oxomanganese Complex: Evaluation of the DFT B3LYP Level of Theory. *J. Chem. Theory Comput.* **2010**, *6*, 755−760.
(16) Kreuer, K. On the Development of Proton Conducting Polymer Membranes for Hydrogen and Methanol Fuel Cells. *J. Membr. Sci.* **2001**, *185*, 29−39.
(17) McEvoy, J. P.; Gascon, J. A.; Batista, V. S.; Brudvig, G. W. The Mechanism of Photosynthetic Water Splitting. *Photochem. Photobiol. Sci.* **2005**, *4*, 940−949.
(18) Sproviero, E. M.; Gascón, J. A.; McEvoy, J. P.; Brudvig, G. W.; Batista, V. S. Computational Studies of the O_2-Evolving Complex of Photosystem II and Biomimetic Oxomanganese Complexes. *Coord. Chem. Rev.* **2008**, *252*, 395−415.
(19) Ho, J.; Kish, E.; Méndez-Hernández, D. D.; WongCarter, K.; Pillai, S.; Kodis, G.; Niklas, J.; Poluektov, O. G.; Gust, D.; Moore, T. A.; Moore, A. L.; Batista, V. S.; Robert, B. Triplet-Triplet Energy Transfer in Artificial and Natural Photosynthetic Antennas. *Proc. Natl. Acad. Sci. U. S. A.* **2017**, *114*, E5513−E5521.
(20) Weller, A. Innermolekularer Protonenübergang im angeregten Zustand. *Z. Elektrochem.* **1956**, *60*, 1144−1147.
(21) Weller, A. Fast Reactions of Excited Molecules. *Prog. React. Kinet. Mech.* **1961**, *1*, 187.
(22) Shizuka, H. Excited-State Proton-Transfer Reactions and Proton-Induced Quenching of Aromatic Compounds. *Acc. Chem. Res.* **1985**, *18*, 141−147.
(23) Formosinho, S. J.; Arnaut, L. G. Excited-State Proton Transfer Reactions II. Intramolecular Reactions. *J. Photochem. Photobiol., A* **1993**, *75*, 21−48.
(24) Ormson, S.; Brown, R. Excited State Intramolecular Proton Transfer. I: ESIPT to Nitrogen. *Prog. React. Kinet.* **1994**, *19*, 45−91.
(25) Le Gourriérec, D.; Ormson, S. M.; Brown, R. G. Excited State Intramolecular Proton Transfer. Part 2: ESIPT to Oxygen. *Prog. React. Kinet.* **1994**, *19*, 211−275.
(26) Elsaesser, T.; Bakker, H. J. *Ultrafast Hydrogen Bonding Dynamics and Proton Transfer Processes in the Condensed Phase*; Springer Science & Business Media, 2013; Vol. *23*.
(27) Balasubramanian, M.; Reynolds, A.; Blair, T. J.; Khalil, M. Probing Ultrafast Vibrational Dynamics of Intramolecular Hydrogen Bonds With Broadband Infrared Pump-Probe Spectroscopy. *Chem. Phys.* **2019**, *519*, 38−44.
(28) Yong, H.; et al. Observation of the Molecular Response to Light Upon Photoexcitation. *Nat. Commun.* **2020**, *11*, 2157.
(29) Yong, H.; et al. Ultrafast X-Ray Scattering Offers a Structural View of Excited-State Charge Transfer. *Proc. Natl. Acad. Sci. U. S. A.* **2021**, *118*, No. e2021714118.
(30) Jay, R. M.; Kunnus, K.; Wernet, P.; Gaffney, K. J. Capturing Atom-Specific Electronic Structural Dynamics of Transition-Metal Complexes With Ultrafast Soft X-Ray Spectroscopy. *Annu. Rev. Phys. Chem.* **2022**, *73*, 187−208.
(31) Yang, J.; et al. Direct Observation of Ultrafast Hydrogen Bond Strengthening in Liquid Water. *Nature* **2021**, *596*, 531−535.
(32) Marx, D.; Tuckerman, M. E.; Hutter, J.; Parrinello, M. The Nature of the Hydrated Excess Proton in Water. *Nature* **1999**, *397*, 601−604.
(33) Vuilleumier, R.; Borgis, D. Transport and Spectroscopy of the Hydrated Proton: A Molecular Dynamics Study. *J. Chem. Phys.* **1999**, *111*, 4251−4266.
(34) Schmitt, U. W.; Voth, G. A. The Computer Simulation of Proton Transfer in Water. *J. Chem. Phys.* **1999**, *111*, 9361−9381.
(35) Marx, D. Proton Transfer 200 Years After von Grotthuss: Insights From ab Initio Simulations. *ChemPhysChem* **2006**, *7*, 1848−1870.
(36) Hassanali, A.; Giberti, F.; Cuny, J.; Kühne, T. D.; Parrinello, M. Proton Transfer Through the Water Gossamer. *Proc. Natl. Acad. Sci. U.S.A.* **2013**, *110*, 13723−13728.
(37) Andot, K.; Hynes, J. T. HCl Acid Ionization in Water - A Theoretical Molecular Modeling. *J. Mol. Liq.* **1995**, *64*, 25−37.
(38) Ando, K.; Hynes, J. T. Acid-Base Proton Transfer and Ion Pair Formation in Solution. *Adv. Chem. Phys.* **1999**, *110*, 381−430.
(39) Park, J. M.; Laio, A.; Iannuzzi, M.; Parrinello, M. Dissociation Mechanism of Acetic Acid in Water. *J. Am. Chem. Soc.* **2006**, *128*, 11318−11319.
(40) Daschakraborty, S.; Kiefer, P. M.; Miller, Y.; Motro, Y.; Pines, D.; Pines, E.; Hynes, J. T. Reaction Mechanism for Direct Proton Transfer from Carbonic Acid to a Strong Base in Aqueous Solution II: Solvent Coordinate-Dependent Reaction Path. *J. Phys. Chem. B* **2016**, *120*, 2281−2290.
(41) Kiefer, P. M.; Hynes, J. T. Theoretical Aspects of Tunneling Proton Transfer Reactions in a Polar Environment. *J. Phys. Org. Chem.* **2010**, *23*, 632−646.
(42) Laermer, F.; Elsaesser, T.; Kaiser, W. Femtosecond Spectroscopy of Excited-State Proton-Transfer in 2-(2'-Hydroxyphenyl)-Benzothiazole. *Chem. Phys. Lett.* **1988**, *148*, 119−124.
(43) Lochbrunner, S.; Wurzer, A. J.; Riedle, E. Ultrafast Excited-State Proton Transfer and Subsequent Coherent Skeletal Motion of 2-(2'-Hydroxyphenyl)benzothiazole. *J. Chem. Phys.* **2000**, *112*, 10699−10702.
(44) Lochbrunner, S.; Wurzer, A. J.; Riedle, E. Microscopic Mechanism of Ultrafast Excited-State Intramolecular Proton Transfer: A 30-fs Study of 2-(2'-Hydroxyphenyl)benzothiazole. *J. Phys. Chem. A* **2003**, *107*, 10580−10590.
(45) Elsaesser, T.; Kaiser, W. Visible and Infrared Spectroscopy of Intramolecular Proton Transfer Using Picosecond Laser Pulses. *Chem. Phys. Lett.* **1986**, *128*, 231−237.
(46) Rini, M.; Dreyer, J.; Nibbering, E. T. J.; Elsaesser, T. Ultrafast Vibrational Relaxation Processes Induced by Intramolecular Excited State Hydrogen Transfer. *Chem. Phys. Lett.* **2003**, *374*, 13−19.
(47) Rini, M.; Kummrow, A.; Dreyer, J.; Nibbering, E. T. J.; Elsaesser, T. Femtosecond Mid-Infrared Spectroscopy of Condensed Phase Hydrogen-Bonded Systems as a Probe of Structural Dynamics. *Faraday Discuss.* **2003**, *122*, 27−40.
(48) Mohammed, O. F.; Luber, S.; Batista, V. S.; Nibbering, E. T. J. Ultrafast Branching of Reaction Pathways in 2-(2'-Hydroxyphenyl)-benzothiazole in Polar Acetonitrile Solution. *J. Phys. Chem. A* **2011**, *115*, 7550−7558.
(49) Luber, S.; Adamczyk, K.; Nibbering, E. T. J.; Batista, V. S. Photoinduced Proton Coupled Electron Transfer in 2-(2'-Hydroxyphenyl)-Benzothiazole. *J. Phys. Chem. A* **2013**, *117*, 5269−5279.
(50) de Vivie-Riedle, R.; De Waele, V.; Kurtz, L.; Riedle, E. Ultrafast Excited-State Proton Transfer of 2-(2'-Hydroxyphenyl)benzothiazole: Theoretical Analysis of the Skeletal Deformations and the Active Vibrational Modes. *J. Phys. Chem. A* **2003**, *107*, 10591−10599.
(51) Huynh, M. H. V.; Meyer, T. J. Proton-Coupled Electron Transfer. *Chem. Rev.* **2007**, *107*, 5004−5064.
(52) Hammes-Schiffer, S.; Stuchebrukhov, A. A. Theory of Coupled Electron and Proton Transfer Reactions. *Chem. Rev.* **2010**, *110*, 6939−6960.
(53) Hammes-Schiffer, S. Proton-Coupled Electron Transfer: Moving Together and Charging Forward. *J. Am. Chem. Soc.* **2015**, *137*, 8860−8871.

https://doi.org/10.1021/acs.jpclett.2c02037
J. Phys. Chem. Lett. 2022, 13, 8254−8263

(54) Josefsson, I.; Kunnus, K.; Schreck, S.; Föhlisch, A.; de Groot, F.; Wernet, P.; Odelius, M. Ab Initio Calculations of X-Ray Spectra: Atomic Multiplet and Molecular Orbital Effects in a Multiconfigurational SCF Approach to the L-Edge Spectra of Transition Metal Complexes. *J. Phys. Chem. Lett.* **2012**, *3*, 3565−3570.
(55) Lopata, K.; Van Kuiken, B. E.; Khalil, M.; Govind, N. Linear-Response and Real-Time Time-Dependent Density Functional Theory Studies of Core-Level Near-Edge X-Ray Absorption. *J. Chem. Theory Comput.* **2012**, *8*, 3284−3292.
(56) Van Kuiken, B. E.; Huse, N.; Cho, H.; Strader, M. L.; Lynch, M. S.; Schoenlein, R. W.; Khalil, M. Probing the Electronic Structure of a Photoexcited Solar Cell Dye with Transient X-Ray Absorption Spectroscopy. *J. Phys. Chem. Lett.* **2012**, *3*, 1695−1700.
(57) Wernet, P.; et al. Orbital-Specific Mapping of the Ligand Exchange Dynamics of $Fe(CO)_5$ in Solution. *Nature* **2015**, *520*, 78−81.
(58) Pertot, Y.; Schmidt, C.; Matthews, M.; Chauvet, A.; Huppert, M.; Svoboda, V.; von Conta, A.; Tehlar, A.; Baykusheva, D.; Wolf, J.-P.; Wörner, H. J. Time-Resolved X-Ray Absorption Spectroscopy With a Water Window High-Harmonic Source. *Science* **2017**, *355*, 264−267.
(59) Attar, A. R.; Bhattacherjee, A.; Pemmaraju, C. D.; Schnorr, K.; Closser, K. D.; Prendergast, D.; Leone, S. R. Femtosecond X-Ray Spectroscopy of an Electrocyclic Ring-Opening Reaction. *Science* **2017**, *356*, 54−58.
(60) Norman, P.; Dreuw, A. Simulating X-Ray Spectroscopies and Calculating Core-Excited States of Molecules. *Chem. Rev.* **2018**, *118*, 7208−7248.
(61) Britz, A.; et al. Using Ultrafast X-Ray Spectroscopy to Address Questions in Ligand-Field Theory: The Excited State Spin and Structure of $[Fe(dcpp)_2]^{2+}$. *Inorg. Chem.* **2019**, *58*, 9341−9350.
(62) Vidal, M. L.; Pokhilko, P.; Krylov, A. I.; Coriani, S. Equation-of-Motion Coupled-Cluster Theory to Model L-Edge X-Ray Absorption and Photoelectron Spectra. *J. Phys. Chem. Lett.* **2020**, *11*, 8314−8321.
(63) Besley, N. A. Modeling of the Spectroscopy of Core Electrons with Density Functional Theory. *Wiley Interdiscip. Rev.: Comput. Mol. Sci.* **2021**, *11*, No. e1527.
(64) Halbert, L.; Vidal, M. L.; Shee, A.; Coriani, S.; Severo Pereira Gomes, A. Relativistic EOM-CCSD for Core-Excited and Core-Ionized State Energies Based on the Four-Component Dirac−Coulomb(−Gaunt) Hamiltonian. *J. Chem. Theory Comput.* **2021**, *17*, 3583−3598.
(65) Tsuru, S.; Vidal, M. L.; Pápai, M.; Krylov, A. I.; Møller, K. B.; Coriani, S. An Assessment of Different Electronic Structure Approaches for Modeling Time-Resolved X-Ray Absorption Spectroscopy. *Struct. Dyn.* **2021**, *8*, 024101.
(66) Segatta, F.; Nenov, A.; Orlandi, S.; Arcioni, A.; Mukamel, S.; Garavelli, M. Exploring the Capabilities of Optical Pump X-Ray Probe NEXAFS Spectroscopy to Track Photo-Induced Dynamics Mediated by Conical Intersections. *Faraday Discuss.* **2020**, *221*, 245−264.
(67) Neville, S. P.; Chergui, M.; Stolow, A.; Schuurman, M. S. Ultrafast X-Ray Spectroscopy of Conical Intersections. *Phys. Rev. Lett.* **2018**, *120*, 243001.
(68) Morzan, U. N.; Videla, P. E.; Soley, M. B.; Nibbering, E. T. J.; Batista, V. S. Vibronic Dynamics of Photodissociating ICN from Simulations of Ultrafast X-Ray Absorption Spectroscopy. *Angew. Chem., Int. Ed.* **2020**, *59*, 20044−20048.
(69) Chen, L. X. Probing Transient Molecular Structures in Photochemical Processes Using Laser-Initiated Time-resolved X-Ray Absorption Spectroscopy. *Annu. Rev. Phys. Chem.* **2005**, *56*, 221−254.
(70) Winter, B.; Faubel, M. Photoemission from Liquid Aqueous Solutions. *Chem. Rev.* **2006**, *106*, 1176−1211.
(71) Bressler, C.; Chergui, M. Molecular Structural Dynamics Probed by Ultrafast X-Ray Absorption Spectroscopy. *Annu. Rev. Phys. Chem.* **2010**, *61*, 263−282.
(72) Milne, C.; Penfold, T.; Chergui, M. Recent Experimental and Theoretical Developments in Time-Resolved X-Ray Spectroscopies. *Coord. Chem. Rev.* **2014**, *277*, 44−68.
(73) Smith, J. W.; Saykally, R. J. Soft X-ray Absorption Spectroscopy of Liquids and Solutions. *Chem. Rev.* **2017**, *117*, 13909−13934.
(74) Scholes, G. D.; et al. Using Coherence to Enhance Function in Chemical and Biophysical Systems. *Nature* **2017**, *543*, 647−656.
(75) Kraus, P. M.; Zürch, M.; Cushing, S. K.; Neumark, D. M.; Leone, S. R. The Ultrafast X-Ray Spectroscopic Revolution in Chemical Dynamics. *Nat. Rev. Chem.* **2018**, *2*, 82−94.
(76) Geneaux, R.; Marroux, H. J.; Guggenmos, A.; Neumark, D. M.; Leone, S. R. Transient Absorption Spectroscopy Using High Harmonic Generation:A Review of Ultrafast X-Ray Dynamics in Molecules and Solids. *Philos. Trans. R. Soc. A* **2019**, *377*, 20170463.
(77) Ekimova, M.; Quevedo, W.; Faubel, M.; Wernet, P.; Nibbering, E. T. J. A Liquid Flatjet System for Solution Phase Soft-X-Ray Spectroscopy. *Struct. Dyn.* **2015**, *2*, 054301.
(78) Fondell, M.; et al. Time-Resolved Soft X-Ray Absorption Spectroscopy in Transmission Mode on Liquids at MHz Repetition Rates. *Struct. Dyn.* **2017**, *4*, 054902.
(79) Bergmann, U.; Kern, J.; Schoenlein, R. W.; Wernet, P.; Yachandra, V. K.; Yano, J. Using X-Ray Free-Electron Lasers for Spectroscopy of Molecular Catalysts and Metalloenzymes. *Nat. Rev. Phys.* **2021**, *3*, 264−282.
(80) Popmintchev, T.; et al. Bright Coherent Ultrahigh Harmonics in the keV X-ray Regime from Mid-Infrared Femtosecond Lasers. *Science* **2012**, *336*, 1287−1291.
(81) Bressler, C.; Milne, C.; Pham, V.-T.; ElNahhas, A.; van der Veen, R. M.; Gawelda, W.; Johnson, S.; Beaud, P.; Grolimund, D.; Kaiser, M.; et al. Femtosecond XANES Study of the Light-Induced Spin Crossover Dynamics in an Iron (II) Complex. *Science* **2009**, *323*, 489−492.
(82) Greene, S. M.; Batista, V. S. Tensor-Train Split-Operator Fourier transform (TT-SOFT) Method: Multidimensional Nonadiabatic Quantum Dynamics. *J. Chem. Theory Comput.* **2017**, *13*, 4034−4042.
(83) Baiardi, A.; Stein, C. J.; Barone, V.; Reiher, M. Optimization of Highly Excited Matrix Product States With an Application to Vibrational Spectroscopy. *J. Chem. Phys.* **2019**, *150*, 094113.
(84) Chen, L.; Gelin, M. F.; Zhao, Y.; Domcke, W. Mapping of Wave Packet Dynamics at Conical Intersections by Time- and Frequency-Resolved Fluorescence Spectroscopy: A Computational Study. *J. Phys. Chem. Lett.* **2019**, *10*, 5873−6880.
(85) Gelin, M. F.; Borrelli, R. Simulation of Nonlinear Femtosecond Signals at Finite Temperature via a Thermo Field Dynamics-Tensor Train Method: General Theory and Application to Time- and Frequency-Resolved Fluorescence of the Fenna-Matthews-Olson Complex. *J. Chem. Theory Comput.* **2021**, *17*, 4316−4331.
(86) Soley, M. B.; Bergold, P.; Gorodetsky, A. A.; Batista, V. S. Functional Tensor-Train Chebyshev Method for Multidimensional Quantum Dynamics Simulations. *J. Chem. Theory Comput.* **2022**, *18*, 25−36.
(87) Soley, M. B.; Bergold, P.; Batista, V. S. Iterative Power Algorithm for Global Optimization with Quantics Tensor Trains. *J. Chem. Theory Comput.* **2021**, *17*, 3280−3291.
(88) Beck, M. H.; Jäckle, A.; Worth, G. A.; Meyer, H.-D. The Multiconfiguration Time-Dependent Hartree (MCTDH) Method: A Highly Efficient Algorithm for Propagating Wavepackets. *Phys. Rep.* **2000**, *324*, 1−105.
(89) Soley, M. B.; Videla, P. E.; Nibbering, E. T. J.; Batista, V. S. *michelinesoley/HBT*; 2022 (https://github.com/michelinesoley/HBT).
(90) Petrone, A.; Lingerfelt, D. B.; Williams-Young, D. B.; Li, X. Ab Initio Transient Vibrational Spectral Analysis. *J. Phys. Chem. Lett.* **2016**, *7*, 4501−4508.
(91) Kim, J.; Wu, Y.; Brédas, J.-L.; Batista, V. S. Quantum Dynamics of the Excited-State Intramolecular Proton Transfer in 2-(2'-Hydroxyphenyl)benzothiazole. *Isr. J. Chem.* **2009**, *49*, 187−197.
(92) Chudoba, C.; Riedle, E.; Pfeiffer, M.; Elsaesser, T. Vibrational Coherence in Ultrafast Excited State Proton Transfer. *Chem. Phys. Lett.* **1996**, *263*, 622−628.

https://doi.org/10.1021/acs.jpclett.2c02037
J. Phys. Chem. Lett. 2022, 13, 8254−8263

(93) de Vivie-Riedle, R.; De Waele, V.; Kurtz, L.; Riedle, E. Ultrafast Excited-State Proton Transfer of 2-(2'-Hydroxyphenyl)benzothiazole: Theoretical Analysis of the Skeletal Deformations and the Active Vibrational Modes. *J. Phys. Chem. A* **2003**, *107*, 10591−10599.
(94) Pfeiffer, M.; Lenz, K.; Lau, A.; Elsaesser, T. Resonance Raman Studies of Heterocyclic Aromatic Compounds Showing Ultrafast Intramolecular Proton Transfer. *J. Raman Spectrosc.* **1995**, *26*, 607−615.
(95) Loe, C. M.; Liekhus-Schmaltz, C.; Govind, N.; Khalil, M. Spectral Signatures of Ultrafast Excited-State Intramolecular Proton Transfer from Computational Multi-edge Transient X-ray Absorption Spectroscopy. *J. Phys. Chem. Lett.* **2021**, *12*, 9840−9847.
(96) Eckert, S.; Miedema, P.; Quevedo, W.; O'Cinneide, B.; Fondell, M.; Beye, M.; Pietzsch, A.; Ross, M.; Khalil, M.; Föhlisch, A. Molecular Structures and Protonation State of 2-Mercaptopyridine in Aqueous Solution. *Chem. Phys. Lett.* **2016**, *647*, 103−106.
(97) List, N. H.; Dempwolff, A. L.; Dreuw, A.; Norman, P.; Martínez, T. J. Probing Competing Relaxation Pathways in Malonaldehyde With Transient X-Ray Absorption Spectroscopy. *Chem. Sci.* **2020**, *11*, 4180−4193.
(98) Sobolewski, A. L.; Domcke, W.; Hättig, C. Photophysics of Organic Photostabilizers. Ab Initio Study of the Excited-State Deactivation Mechanisms of 2-(2'-Hydroxyphenyl)benzotriazole. *J. Phys. Chem. A* **2006**, *110*, 6301−6306.
(99) Sobolewski, A. L.; Domcke, W. Computational Studies of the Photophysics of Hydrogen-Bonded Molecular Systems. *J. Phys. Chem. A* **2007**, *111*, 11725−11735.
(100) Coe, J. D.; Levine, B. G.; Martínez, T. J. Ab Initio Molecular Dynamics of Excited-State Intramolecular Proton Transfer Using Multireference Perturbation Theory. *J. Phys. Chem. A* **2007**, *111*, 11302−11310.
(101) Chai, J.-D.; Head-Gordon, M. Long-Range Corrected Hybrid Density Functionals with Damped Atom−Atom Dispersion Corrections. *Phys. Chem. Chem. Phys.* **2008**, *10*, 6615−6620.
(102) Dunning, T. H. Gaussian Basis Sets for Use in Correlated Molecular Calculations. I. The Atoms Boron Through Neon and Hydrogen. *J. Chem. Phys.* **1989**, *90*, 1007−1023.
(103) Frisch, M. J.; et al. *Gaussian 16*, rev. C.01; Gaussian Inc.: Wallingford, CT, 2016.
(104) Cancès, E.; Mennucci, B.; Tomasi, J. A New Integral Equation Formalism for the Polarizable Continuum Model: Theoretical Background and Applications to Isotropic and Anisotropic Dielectrics. *J. Chem. Phys.* **1997**, *107*, 3032−3041.
(105) Mennucci, B.; Cancès, E.; Tomasi, J. Evaluation of Solvent Effects in Isotropic and Anisotropic Dielectrics and in Ionic Solutions with a Unified Integral Equation Method: Theoretical Bases, Computational Implementation, and Numerical Applications. *J. Phys. Chem. B* **1997**, *101*, 10506−10517.
(106) Tomasi, J.; Mennucci, B.; Cancès, E. The IEF Version of the PCM Solvation Method: An Overview of a New Method Addressed to Study Molecular Solutes at the QM ab Initio Level. *J. Mol. Struct.: THEOCHEM* **1999**, *464*, 211−226.
(107) Cossi, M.; Scalmani, G.; Rega, N.; Barone, V. New Developments in the Polarizable Continuum Model for Quantum Mechanical and Classical Calculations on Molecules in Solution. *J. Chem. Phys.* **2002**, *117*, 43−54.
(108) Tomasi, J.; Mennucci, B.; Cammi, R. Quantum Mechanical Continuum Solvation Models. *Chem. Rev.* **2005**, *105*, 2999−3094.
(109) Miller, W. H.; Handy, N. C.; Adams, J. E. Reaction Path Hamiltonian for Polyatomic Molecules. *J. Chem. Phys.* **1980**, *72*, 99−112.
(110) Carrington, T.; Miller, W. H. Reaction Surface Hamiltonian for the Dynamics of Reactions in Polyatomic Systems. *J. Chem. Phys.* **1984**, *81*, 3942−3950.
(111) Carrington, T.; Miller, W. H. Reaction Surface Description of Intramolecular Hydrogen Atom Transfer in Malonaldehyde. *J. Chem. Phys.* **1986**, *84*, 4364−4370.
(112) Pijeau, S.; Foster, D.; Hohenstein, E. G. Excited-State Dynamics of 2-(2'-Hydroxyphenyl)benzothiazole: Ultrafast Proton Transfer and Internal Conversion. *J. Phys. Chem. A* **2017**, *121*, 4595−4605.
(113) Kim, J.; Kim, C. H.; Burger, C.; Park, M.; Kling, M. F.; Kim, D. E.; Joo, T. Non-Born−Oppenheimer Molecular Dynamics Observed by Coherent Nuclear Wave Packets. *J. Phys. Chem. Lett.* **2020**, *11*, 755−761.
(114) Oseledets, I. *oseledets/TT-Toolbox*; 2020 (https://www.github.com/oseledets/TT-Toolbox).
(115) Oseledets, I.; Tyrtyshnikov, E. T. TT-Cross Approximation for Multidimensional Arrays. *Linear Algebra Its Appl.* **2010**, *432*, 70−88.
(116) Gilbert, A. T. B.; Besley, N. A.; Gill, P. M. W. Self-Consistent Field Calculations of Excited States Using the Maximum Overlap Method (MOM). *J. Phys. Chem. A* **2008**, *112*, 13164−13171.
(117) Barca, G. M. J.; Gilbert, A. T. B.; Gill, P. M. W. Simple Models for Difficult Electronic Excitations. *J. Chem. Theory Comput.* **2018**, *14*, 1501−1509.
(118) Dreuw, A.; Head-Gordon, M. Single-Reference ab Initio Methods for the Calculation of Excited States of Large Molecules. *Chem. Rev.* **2005**, *105*, 4009−4037.
(119) Shao, Y.; Gan, Z.; Epifanovsky, E.; Gilbert, A. T.B.; Wormit, M.; Kussmann, J.; Lange, A. W.; Behn, A.; Deng, J.; Feng, X.; Ghosh, D.; Goldey, M.; Horn, P. R.; Jacobson, L. D.; Kaliman, I.; Khaliullin, R. Z.; Kus, T.; Landau, A.; Liu, J.; Proynov, E. I.; Rhee, Y. M.; Richard, R. M.; Rohrdanz, M. A.; Steele, R. P.; Sundstrom, E. J.; Woodcock, H. L.; Zimmerman, P. M.; Zuev, D.; Albrecht, B.; Alguire, E.; Austin, B.; Beran, G. J. O.; Bernard, Y. A.; Berquist, E.; Brandhorst, K.; Bravaya, K. B.; Brown, S. T.; Casanova, D.; Chang, C.-M.; Chen, Y.; Chien, S. H.; Closser, K. D.; Crittenden, D. L.; Diedenhofen, M.; DiStasio, R. A.; Do, H.; Dutoi, A. D.; Edgar, R. G.; Fatehi, S.; Fusti-Molnar, L.; Ghysels, A.; Golubeva-Zadorozhnaya, A.; Gomes, J.; Hanson-Heine, M. W.D.; Harbach, P. H.P.; Hauser, A. W.; Hohenstein, E. G.; Holden, Z. C.; Jagau, T.-C.; Ji, H.; Kaduk, B.; Khistyaev, K.; Kim, J.; Kim, J.; King, R. A.; Klunzinger, P.; Kosenkov, D.; Kowalczyk, T.; Krauter, C. M.; Lao, K. U.; Laurent, A. D.; Lawler, K. V.; Levchenko, S. V.; Lin, C. Y.; Liu, F.; Livshits, E.; Lochan, R. C.; Luenser, A.; Manohar, P.; Manzer, S. F.; Mao, S.-P.; Mardirossian, N.; Marenich, A. V.; Maurer, S. A.; Mayhall, N. J.; Neuscamman, E.; Oana, C. M.; Olivares-Amaya, R.; O'Neill, D. P.; Parkhill, J. A.; Perrine, T. M.; Peverati, R.; Prociuk, A.; Rehn, D. R.; Rosta, E.; Russ, N. J.; Sharada, S. M.; Sharma, S.; Small, D. W.; Sodt, A.; Stein, T.; Stuck, D.; Su, Y.-C.; Thom, A. J.W.; Tsuchimochi, T.; Vanovschi, V.; Vogt, L.; Vydrov, O.; Wang, T.; Watson, M. A.; Wenzel, J.; White, A.; Williams, C. F.; Yang, J.; Yeganeh, S.; Yost, S. R.; You, Z.-Q.; Zhang, I. Y.; Zhang, X.; Zhao, Y.; Brooks, B. R.; Chan, G. K.L.; Chipman, D. M.; Cramer, C. J.; Goddard, W. A.; Gordon, M. S.; Hehre, W. J.; Klamt, A.; Schaefer, H. F.; Schmidt, M. W.; Sherrill, C. D.; Truhlar, D. G.; Warshel, A.; Xu, X.; Aspuru-Guzik, A.; Baer, R.; Bell, A. T.; Besley, N. A.; Chai, J.-D.; Dreuw, A.; Dunietz, B. D.; Furlani, T. R.; Gwaltney, S. R.; Hsu, C.-P.; Jung, Y.; Kong, J.; Lambrecht, D. S.; Liang, W.; Ochsenfeld, C.; Rassolov, V. A.; Slipchenko, L. V.; Subotnik, J. E.; Van Voorhis, T.; Herbert, J. M.; Krylov, A. I.; Gill, P. M.W.; Head-Gordon, M. Advances in Molecular Quantum Chemistry Contained in the Q-Chem 4 Program Package. *Mol. Phys.* **2015**, *113*, 184−215.

https://doi.org/10.1021/acs.jpclett.2c02037
J. Phys. Chem. Lett. 2022, 13, 8254−8263